International Organization of Research & Development (IORD)
ISSN: 2348-0831
Vol 13 Special Issue 02 | 2026

Synthesis and Structural study of Cerium Ferrite Semiconductor

Bhanudas V Narwade[1], Dr. Pravin A Murade[2], Dr. Rajesh R. Raut[3]
[1]*Physics Department, Rajshri Shahu College of Engineering, Buldhana, Maharashtra, India*
[2]*RDIK & KD College, Badnera, Amravati, Maharashtra, India*
[3]*Science and Humanities Department, Sanmati Engineering College, Washim, Maharashtra, India*

DOI: 10.5281/zenodo.19537785

ABSTRACT

In this research work, Cerium ferrite ($CeFeO_3$) nanoparticles were synthesized using a sol–gel auto-combustion method employing cerium nitrate hexahydrate, ferric nitrate nonahydrate and citric acid as precursor materials. The precursor solutions were mixed and stirred at 80°C and the pH of the solution was adjusted to ~7 using ammonia to promote hydrolysis and complex formation. Ethylene glycol was added as a polymerization agent to facilitate the formation of a stable sol–gel network. The obtained gel was dried to initiate a self-combustion process, producing a precursor powder that was further calcined at 760°C for 12 h to obtain crystalline cerium ferrite. The structural properties of the synthesized sample were investigated using X-ray diffraction (XRD) analysis. The XRD pattern exhibited broad diffraction peaks, confirming the nanocrystalline nature of the material. The major diffraction peaks correspond to the orthorhombic perovskite structure of $CeFeO_3$ and agree well with the standard JCPDS card No. 00-022-0166. A weak peak at $2\theta \approx 28.75°$ indicated the presence of a minor CeO_2 secondary phase. The average crystallite size calculated using the Scherrer equation was found to be in the range of 13 nm. The calculated lattice parameters and unit cell volume confirm the formation of orthorhombic cerium ferrite structure.

Keywords: - cerium ferrite, XRD, sol-gel, Nanomaterial, composite

1.INTRODUCTION

Multiferroic materials have gained significant attention because they exhibit multiple ferroic order parameters, such as ferroelectricity, ferromagnetism and ferroelasticity, within a single phase. The coexistence of these properties leads to magnetoelectric coupling, enabling control of magnetic properties through electric fields. Due to these characteristics, multiferroic materials are widely investigated for applications in data storage devices, sensors, actuators, spintronics and photocatalysis [1–3]. Ferrite-based materials are particularly important among multiferroics because of their chemical stability, moderate magnetic properties, high electrical resistivity and low production cost, making them suitable for electronic, magnetic and catalytic applications [4]. Their properties can be further enhanced through doping and optimized
synthesis methods such as sol–gel, hydrothermal and solid-state techniques [5–7]. Recent studies have shown that rare-earth and transition metal co-doping improves the multifunctional properties of ferrites. In particular, the incorporation of cerium ions in nickel, chromium and bismuth ferrites enhances magnetic ordering, dielectric behavior and electrical conductivity. Moreover, cerium-doped ferrites exhibit improved magnetic and electrical responses under visible light irradiation, highlighting their potential for photocatalytic and optoelectronic applications [8,9]. Environmental pollution caused by industrial wastewater is a serious global issue, as it contains toxic organic compounds harmful to ecosystems and human health. Conventional treatment methods such as biological, chemical and physical processes often suffer from high energy consumption and may produce secondary pollutants. Therefore, the development of efficient and environmentally friendly materials for pollutant degradation has become an important research focus [10–11]. Nanostructured ferrites and iron-based oxides have attracted considerable attention because of their chemical stability, catalytic activity and magnetic separability, which enable easy recovery and reuse in environmental remediation processes [12–13]. Among these materials, perovskite ferrites with the general formula ABO_3 exhibit tunable physicochemical properties and strong photocatalytic activity under visible light irradiation [14].
A notable subgroup is lanthanide orthoferrites ($AFeO_3$), where A represents a rare-earth element. These materials show promising magnetic, electrical and catalytic properties and are widely investigated for applications in catalysis, semiconductors, electrochemical systems, biomedical technologies and hydrogen production [15–16]. Lanthanide orthoferrites can be synthesized through several methods, including solid-state reactions, hydrothermal processes, and sol–gel techniques, with the sol–gel method offering better control over stoichiometry, particle size and phase purity [17–19]. However, the synthesis of cerium ferrite ($CeFeO_3$) is challenging because Ce^{3+} ions easily oxidize to Ce^{4+}, leading to the formation of a stable CeO_2 phase [20].

Nevertheless, controlled calcination can produce $CeFeO_3$ nanostructures, sometimes accompanied by a CeO_2 phase that enhances photocatalytic performance [21–23]. $CeFeO_3$ typically exhibits weak ferromagnetic or paramagnetic behavior, although doping with elements such as silver can enhance its magnetic properties and improve catalyst recovery [24–27]. In addition, lanthanide orthoferrites have shown potential in energy storage applications due to their redox activity and high specific capacitance. For instance, Nd-doped $SmFeO_3$ electrodes exhibit high capacitance and excellent cyclic stability [28], while $CeFeO_3/CeO_2/Fe_2O_3$ composites display pseudocapacitive behavior with efficient charge transfer characteristics [29-30].
Therefore, the present study focuses on the sol–gel synthesis of $CeFeO_3$ and the investigation of its structural properties for potential multifunctional applications.

2. EXPERIMENT METHOD

All chemicals used in the present work were of analytical grade and were used without any further purification. Stoichiometric amounts of cerium nitrate hexahydrate ($Ce(NO_3)_3{\cdot}6H_2O$), ferric nitrate nonahydrate ($Fe(NO_3)_3{\cdot}9H_2O$) and citric acid ($C_6H_8O_7$) were used as starting precursors. (Fig 1) Each chemical was initially dissolved separately in deionized water to form clear solutions. The prepared precursor solutions were then mixed together and subjected to continuous magnetic stirring at 80°C for 30 min to ensure complete dissolution and homogeneity of the reactants. After achieving a uniform solution, ammonia (NH_3) solution was slowly added dropwise in order to adjust the pH to approximately 7, which facilitated the hydrolysis process and promoted complex formation among the metal ions. Subsequently, ethylene glycol was added to the reaction mixture to act as a polymerization agent and promote the formation of a stable sol–gel network. The resulting solution was further heated at 80°C under constant magnetic stirring for about 2 h, leading to the gradual transformation of the solution into a black-colored viscous gel. The obtained gel was then dried at 140°C, which initiated a self-propagating combustion process. During this stage, most of the organic components were decomposed and removed, resulting in the formation of a brown precursor powder of cerium ferrite. The obtained powder was then ground using a mortar and pestle for approximately 30 min to achieve fine particle size and improve homogeneity. Finally, the ground powder was calcined (sintered) in a muffle furnace at 760°C for 12 h to obtain the desired crystalline cerium ferrite material.

3. RESULTS AND DISCUSSION

3.1. Structural analysis

The structural properties of the synthesized cerium ferrite samples were investigated using X-ray diffraction (XRD) analysis. The obtained XRD pattern shows relatively broad diffraction peaks, indicating the nanocrystalline nature of the synthesized material.
The diffraction pattern (Fig. 2) exhibits prominent peaks at 2θ values of 32.92°, 47.67°, 57.59°, 68.36° and 77.03°, which correspond to the crystallographic planes (112), (221), (024),
(041) and (116) respectively. These peaks are consistent with the standard JCPDS card No. 00-022-0166, confirming the formation of cerium ferrite with an orthorhombic perovskite crystal structure. The obtained results indicate that the crystal structure of the prepared samples remains stable without significant structural changes. The major diffraction peaks corresponding to the planes (110), (112) and (221) were further analyzed to understand the lattice characteristics of cerium ferrite [31, 32]. A weak diffraction peak observed at $2\theta \approx 28.75°$, corresponding to the
(110) plane, suggests the presence of a small amount of CeO_2 secondary phase. Similar observations have been reported for cerium ferrite synthesized at different calcination temperatures [33, 34].
Apart from this minor peak, no additional impurity peaks were observed, indicating that the synthesized sample is predominantly phase-pure cerium ferrite. A similar orthorhombic phase of cerium ferrite synthesized through the co-precipitation method has also been reported
by Manjula et al. [35]. The average crystallite size of the synthesized material was estimated using the Scherrer equation:

$$D = \frac{k\lambda}{\beta \cos\theta} \quad \text{----------} (1)$$

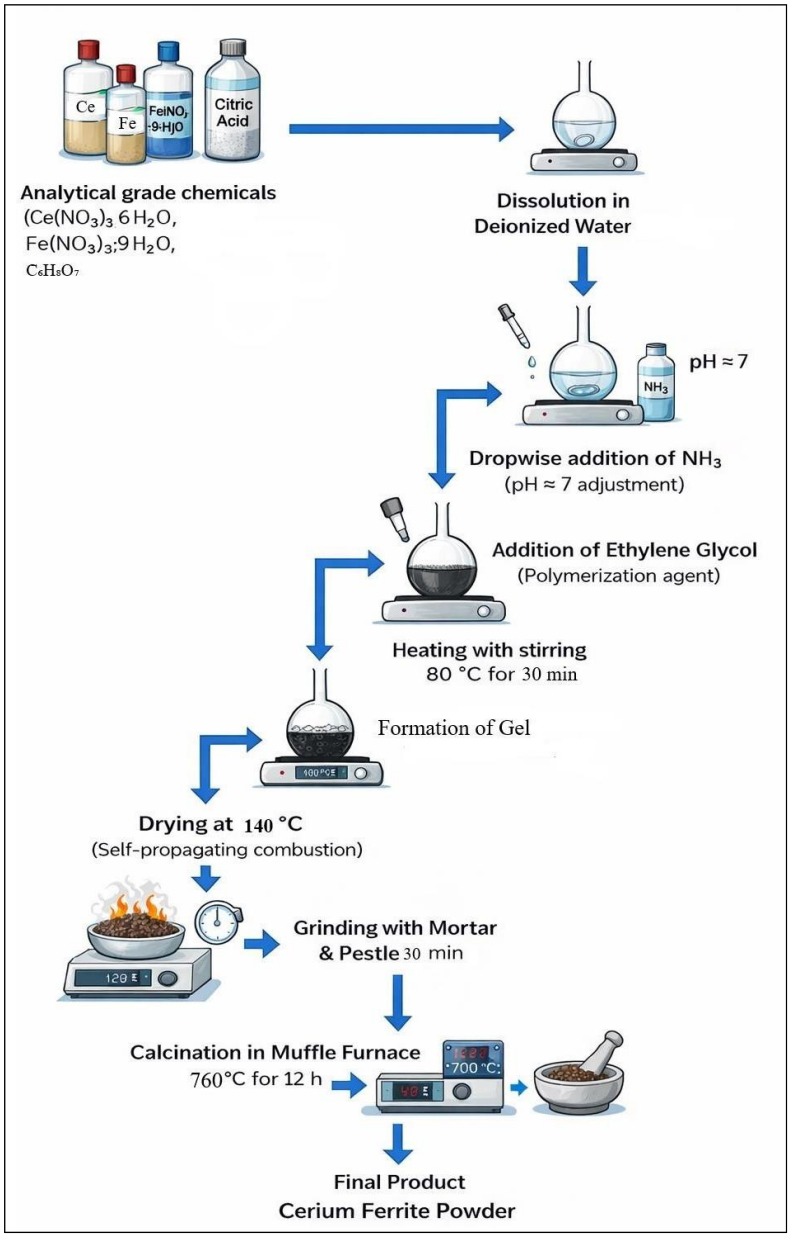

Fig 1 Experimental procedure of cerium ferrite synthesis

Where k is the Scherrer constant (0.94), λ represents the wavelength of the incident X-ray radiation, β is the full width at half maximum expressed in radians and θ is the Bragg diffraction angle. Using this relation, the crystallite size of the prepared samples was found to be in the
range of 13-15 nm, confirming the nanoscale nature of the material. These results are in good agreement with previously reported studies [36].

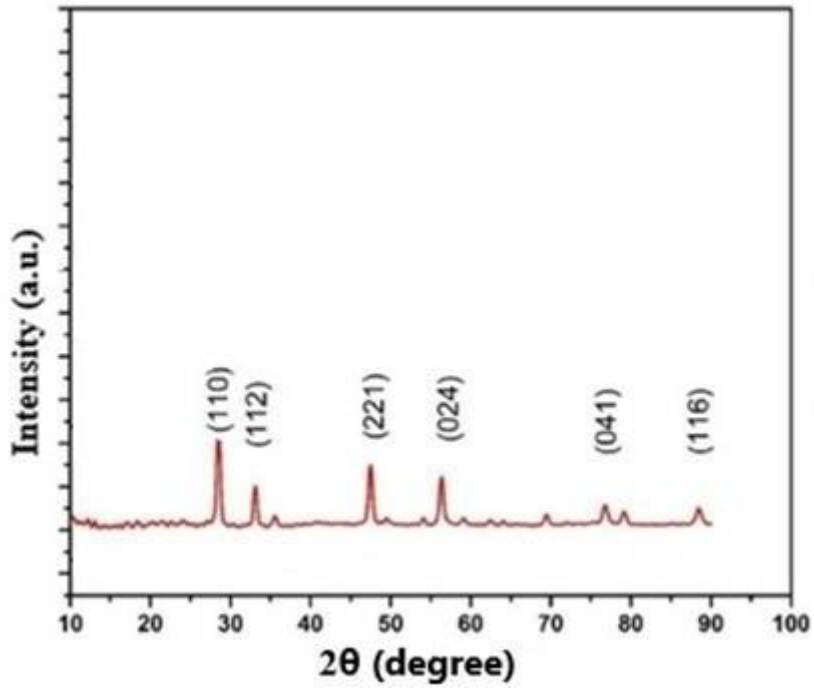

Fig 2- XRD of cerium ferrite composite

The structural parameters of cerium ferrite were further calculated from the XRD data and are presented in Table 1. The lattice constants a, b and c were determined using the relation:

$$\frac{1}{d^2} = \frac{h^2}{a^2} + \frac{k^2}{b^2} + \frac{l^2}{c^2} \quad \text{----------(2)}$$

where h, k and l represent the Miller indices of the corresponding diffraction planes [37]. Using the calculated lattice constants, the unit cell volume was also determined and listed in Table 1 [38]. The obtained lattice parameters are consistent with the orthorhombic crystal structure and are in good agreement with previously reported values by Ananthraman et al [39].

Table 1 - lattice constant and crystallite size of cerium ferrite composite

Sample	a (Å)	b (Å)	c (Å)	Cell Volume (Å³)
CeFeO3	5.625	5.499	7.92	245

4. CONCLUSION

In conclusion, Cerium ferrite ($CeFeO_3$) nanoparticles were successfully synthesized using the sol–gel method. X-ray diffraction analysis confirmed the formation of an orthorhombic perovskite crystal structure consistent with standard JCPDS data. The broad diffraction peaks
indicated the nanocrystalline nature of the synthesized material. The average crystallite size calculated using the Scherrer equation was found to be in the range of 13-15 nm with a small amount of CeO_2 secondary phase. These results demonstrate that the adopted synthesis method is effective for producing nanostructured cerium ferrite with stable structural properties.

5. REFERENCES

[1] Lee J, Oh J, Lee J, Choi S., Journal of Magnetic Materials, 2004;272:2230–2.
[2] Harris V. G., IEEE Transactions on Magnetics,2011;48(3):1075–104.
[3] Akhtar M.N., Yousaf M., Khan S., Nazir M., Ahmad M., Khan M.A., Ceramic International, 2017; 43 (18) : 17032–40.
[4] Kum J.S., Kim S.J., Shim I-B, Kim C.S., Journal of Magnetic Materials, 2004;272:2227–9.
[5] Mandal S, Phadtare S, Sastry M., Current Applied Physics, 2005;5(2):118–27.
[6] Menzer G. XX. Die kristallstruktur der granate. Z. Kristallogr. Cryst. Mater 1929;69 (1–6):300–96.

[7] Gilleo M, Geller S., Physics Review, 1958;110(1):73.
[8] Jiaqian W, Jian Y, Yulong J, Tai Q., J. Rare Earths 2011;29(6): 562–6.
[9] Wickersheim K, Buchanan R., J Applied Physics, 1967;38(3):1048–9.
[10] Chetkin M, Morozova I, Tyutneva G., U. Soviet PhysicsSolid State, 1968;9:2852.
[11] M.N.H. Mia, M.F. Pervez, M.K. Hossain, M.R. Rahman, M.J. Uddin, M.A. A Mashud, H.K. Ghosh, M. Hoq, Results Phys. 7 (2017) 2683–2691.
[12] J. Ding, J. Ming, D. Lu, W. Wu, M. Liu, X. Zhao, C. Li, M. Yang, P. Fang, Catal. Sci. Technol. 7 (2017) 2283–2297.
[13] L. Li, F. Wang, J. Feng, S. Guo, M. Xu, L. Wang, G. Quan, J. Mater. Sci. Mater. Electron. 32 (2021) 16400–16410.
[14] A.N. Matveyeva, S.O. Omarov, M.A. Gavrilova, D.A. Sladkovskiy, D.Y. Murzin, Materials 15 (2022) 7970.
[15] A. Mishra, N. Priyadarshini, S. Mansingh, K. Parida, Adv. Colloid Interface Sci. (2024) 103300.
[16] N. Lin, F. Sheng, X. Chen, X. Hu, N. Zhuang, J. Rare Earths 41 (2023) 2018–2024.
[17] M. Imtiaz, S. Gouadria, A.G. Al-Sehemi, A. Kumar, Inorg. Chem. Commun. 172 (2025) 113680.
[18] W. Azouzi, W. Sigle, H. Labrim, M. Benaissa,Mater. Sci. Semicond. Process. 104 (2019) 104682.
[19] L. Hou, L. Shi, J. Zhao, S. Zhou, S. Pan, X. Yuan, Y. Xin, J. Alloys Compd. 797 (2019) 363–369.
[20] C. Zhang, M. Shang, M. Liu, T. Zhang, L. Ge, H. Yuan, S. Feng, J. Alloys Compd. 665 (2016) 152–157.
[21] L.L. Petschnig, G. Fuhrmann, D. Schildhammer, M. Tribus, H. Schottenberger, H. Huppertz, Ceram. Int. 42 (2016) 4262–4267.
[22] K. Pournemati, A. Habibi-Yangjeh, S.R. Pouran, A. Khataee, Ceram. Int. 48 (2022) 22352– 22361.
[23] B. Wijaya, D.O.B. Apriandanu, R.M. Surya, Y. Yulizar, N.S. Sambudi, M. Khalil, A. Umar, Applied Surface Science Advances 21 (2024) 100599.
[24] A. Javaid, M. Imran, F. Kanwal, S. Latif, M.F. Erben, S. Noureen, Mater. Chem. Phys. 291 (2022) 126704.
[25] P. Desai, A.A. Athawale, Def. Sci. J. 63 (2013).
[26] E.E. Ateia, B. Hussein, C. Singh, M. Arman, The European Physical Journal Plus 137 (2022) 443
[27] L. Hou, L. Shi, J. Zhao, S. Zhou, S. Pan, X. Yuan, Y. Xin, Journal of Alloys and Compounds, 797 (2019) 363–369.
[28] Z. Li, W. Zhang, C. Yuan, Y. Su, RSC Advances, 7 (2017) 12931–12937.
[29] M. Imtiaz, S. Gouadria, A.G. Al-Sehemi, A. Kumar, Inorganic Chemistry Communications, 172 (2025) 113680.
[30] M. Kanimozhi, R. Harikrishnan, M. Mani, S. Kumaresan, A. Rajasekar, N.S. Devi, S. G. Radhakrishnan, L. Sibali, K. Kaviyarasu, Luminescence, 39 (2024) e70009.
[31] K.L. Routray, D. Sanyal, D. Behera, Journal of Applied Physics, 122 (22) (2017), 224104.
[32] N. Pushpa, M. Kokila, Journal of Luminescence, 190 (2017) 100–107
[33] S. Jabbarzare, M. Abdellahi, H. Ghayour, A. Arpanahi, A. Khandan, Journal of Alloys and Compounds, 694 (2017) 800–807
[34] S. Jabbarzare, M. Abdellahi, H. Ghayour, A. Arpanahi, A. Khandan, Journal of Alloys and Compounds, 694 (2017) 800–807
[35] N. Manjula, S. Pulikkutty, T.-W. Chen, S.-M. Chen, X. Liu, Colloids and Surfaces A: Physicochemical and Engineering Aspects, 627 (2021) 127129.
[36] A. Anantharaman, B.A. Josephine, V.M. Teresita, T. Ajeesha, M. George, Journal of Nanoscience and Nanotechnology, 19 (8) (2019) 5116–5129.
[37] M. Pooladi, H. Shokrollahi, S. Lavasani, H. Yang, Materials Chemistry and Physics, 229 (2019) 39–48
[38] S.A. Salman, F.I. Hussain, N.A. Bakr, International Journal of Nanotechnology and Advanced Material, 4 (2016) 1–7.
[39] A. Anantharaman, T. Ajeesha, J. Baby, M. George, Solid State Science, 99 (2020), 105846.